Mechanical Engineering – Scientific Journal, Vol. **44,** No. 1, pp. 5–15 (2026)
Number of article: 700
Received: April 20, 2026
Accepted: May 12, 2026
In print: ISSN 1857–5293
On line: ISSN 1857–9191
UDC: [533.6:004.942]:621.548-42
https://doi.org/10.55302/MESJ2644105s

Original scientific paper

NUMERICAL INVESTIGATION OF AERODYNAMIC EFFICIENCY IN AN AIRFOIL TANDEM CONFIGURATION

Haritina Sakova[1*], Marija Lazarevikj[2], Zoran Markov[2]

[1]*Department of Aerospace Science and Technology, Politecnico di Milano, Italy*
[2]*Faculty of Mechanical Engineering, "Ss. Cyril and Methodius" University in Skopje, North Macedonia*
haritina.sakova@mail.polimi.it, //marija.lazarevikj@mf.edu.mk

A b s t r a c t: Tandem airfoils, used in the fields of aerodynamics for race cars and aircraft designs, are a key part of current research due to the aerodynamic complexity they introduce, while offering performance benefits. A numerical 2D CFD analysis of a tandem airfoil system was performed in this paper to determine their optimal positioning for achieving maximum aerodynamic efficiency and analyzing the resulting flow field. Simulations were conducted in Ansys Fluent using a high-quality mesh and refined boundary layer conditions, targeting $y^+ < 1$. Key parameters analyzed include the lift coefficient C_L, drag coefficient C_D, the C_L/C_D ratio, and flow visualizations such as pressure, velocity, streamlines, velocity vectors, and turbulent kinetic energy. Results indicate that the optimal angle of attack for the variable airfoil is −25°, where the highest C_L/C_D ratio is obtained. However, flow visualizations show wake formation at this angle, highlighting the need for further aerodynamic optimization to balance efficiency and wake reduction.

Key words: aerodynamic optimization; airfoils; CFD 2D analysis; numerical modeling

НУМЕРИЧКО МОДЕЛИРАЊЕ НА АЕРОДИНАМИЧНА ЕФИКАСНОСТ ЗА КОНФИГУРАЦИЈА НА ТАНДЕМ АЕРОДИНАМИЧНИ ПРОФИЛИ

А п с т р а к т: Тандемот на аеродинамичните профили, кои се користат во областа на аеродинамика за тркачки автомобили и за дизајн на авиони, е клучен дел од сегашни истражувања, поради аеродинамичната комплексност што ја создава. Во овој труд е извршена нумеричка анализа 2D CFD на систем од два аеродинамични профила, со цел да се дефинира нивната оптимална заемна поставеност за највисока аеродинамична ефикасност, а притоа да се опфати квалитетот на добиената струјна слика. Симулациите се спроведени со софтверскиот пакет Ansys Fluent, користејќи соодветна дискретизација и услови на граничен слој, со цел воспоставување вредност на $y^+ < 1$. Клучни параметри кои се предмет на анализата се коефициентот на подигање C_L, коефициентот на отпор C_D, односот C_L/C_D, струјната слика на притисокот, интензитетот на брзината, струјните линии, векторското поле на брзина, како и турбулентната кинетичка енергија. Резултатите покажуваат дека оптималниот агол на напад за променливиот аеродинамичен профил е −25°, при што се добива највисок C_L/C_D однос. Покрај тоа, струјните слики покажуваат формирање вртлози при оваа конфигурација, истакнувајќи ја потребата од понатамошна аеродинамична оптимизација, со цел балансирање на ефикасноста и намалување на отпорот кој е резултат на вртложното струење.

Клучни зборови: аеродинамична оптимизација; аеродинамични профили; анализа CFD 2D; нумеричко моделирање

1. INTRODUCTION

Computational Fluid Dynamics (CFD) has been developed as a scientific field by combining the laws of physics, numerical mathematics, and computer science in order to simulate flow phenomena that are difficult to obtain analytically [1, 2]. Its development has accelerated with the availability of powerful processors and advanced numerical methods, which enabled the solution of increasingly complex two-dimensional and three-dimensional flow problems [3, 4]. Later advances in viscous-flow simulation, based on the Navier–Stokes equations, led to the development of turbulence models

with different levels of complexity and accuracy [5]. Aerodynamics studies the forces and motion of bodies moving through air. In engineering analysis, CFD enables numerical simulation of airflow around aerodynamic bodies and provides a detailed representation of the resulting flow field. In this way, it becomes possible to interpret quantities such as velocity, pressure, wake development, and turbulence intensity around a profile or a multi-element configuration [6, 7].

Tandem airfoils are a configuration of two airfoils one behind the other along the flow direction, so the rear airfoil operates in the wake region of the front one [8]. They are used in many race car applications [9], as well as in modern aircraft designs [10]. Compared to a single airfoil, they have shown some efficiency improvements, while also introducing some trade-off decisions when designing this more complex aerodynamic system [11, 12, 13]. In addition to the pressure and velocity distributions generated around each element, the interaction between elements introduces wake effects, local flow separation, and increased turbulence [14]. These effects must be considered simultaneously when evaluating the overall aerodynamic response of the system. Previous numerical studies showed that the relative positioning of tandem airfoils significantly affects lift, drag, and wake interaction, making geometric optimization a key aspect of tandem-airfoil design. The present study is focused on a tandem airfoil configuration composed of NACA 6412 profiles. The usual angle of attack between them is below 30° [15]. One airfoil remains fixed, while the second is treated as a variable element whose angle of attack is changed in order to determine the most favorable relative arrangement. The analysis is based on two-dimensional RANS CFD simulations, as suggested by current literature [16] and includes evaluation of C_L, C_D, y^+, velocity field, pressure field, turbulent kinetic energy, streamlines, and velocity vectors. The goal is to identify the configuration that provides the most favorable aerodynamic response while also assessing the quality of the resulting flow field.

2. THEORETICAL BACKGROUND

2.1. *Governing equations*

The numerical analysis is based on the governing equations of fluid flow solved in ANSYS Fluent [17]. For viscous flow, the study is grounded in the Navier-Stokes formulation, while turbulence is modeled through the Reynolds averaged Navier-Stokes (RANS) approach. The RANS equation used as the basis of the turbulence model is:

$$\frac{\partial(\rho v_i)}{\partial t} + \frac{\partial(\rho v_i v_j)}{\partial x_j} = \\ = -\frac{\partial P}{\partial x_i} + \frac{\partial}{\partial x_j}\left[\mu\left(\frac{\partial v_i}{\partial x_j} + \frac{\partial v_j}{\partial x_i}\right) - \rho\overline{u_i' u_j'}\right] \quad (1)$$

where v_i is the mean flow velocity, u_i' are the velocity fluctuations, μ is the dynamic viscosity, and $-\rho\overline{u_i' u_j'}$ is the Reynolds stress tensor. Using the eddy-viscosity hypothesis, the Reynolds stresses are expressed as:

$$-\rho\overline{u_i' u_j'} = \mu_t\left(\frac{\partial v_i}{\partial x_j} + \frac{\partial v_j}{\partial x_i} - \frac{2}{3}\frac{\partial v_k}{\partial x_k}\delta_{ij}\right) - \frac{2}{3}\rho k\delta_{ij} \quad (2)$$

where μ_t is the turbulent viscosity, k is the turbulent kinetic energy, and δ_{ij} is the Kronecker delta.

2.2. *Realizable k- ε turbulence model*

For the present flow problem, the realizable k-ε model was selected because it is appropriate for simulations involving strong pressure gradients, possible flow separation, merging flow regions, asymmetry, and complex curved flow paths [18]. These characteristics are consistent with the expected flow around the tandem airfoil system.

The transport equation for turbulent kinetic energy is written as:

$$\frac{\partial(\rho k)}{\partial t} + \frac{\partial(\rho U_i k)}{\partial x_i} = \\ = \frac{\partial}{\partial x_j}\left[\left(\mu + \frac{\mu_t}{\sigma_k}\right)\frac{\partial k}{\partial x_j}\right] + P_k + P_b - \rho\varepsilon + S_k \quad (3)$$

The transport equation for the rate of turbulent dissipation is:

$$\frac{\partial(\rho\varepsilon)}{\partial t} + \frac{\partial(\rho U_i \varepsilon)}{\partial x_i} = \frac{\partial}{\partial x_j}\left[\left(\mu + \frac{\mu_t}{\sigma_\varepsilon}\right)\frac{\partial \varepsilon}{\partial x_j}\right] + \\ + \rho C_1 S_\varepsilon - C_2\rho\frac{\varepsilon^2}{k+\sqrt{\nu\varepsilon}} + C_1 C_3 \frac{\varepsilon}{k} P_b + S_\varepsilon \quad (4)$$

The turbulent viscosity is evaluated from:

$$\mu_t = C_\mu \rho \frac{k^2}{\varepsilon} \quad (5)$$

The model constants used are those generally accepted from Launder and Sharma [19].

2.3. *Aerodynamic coefficients and mesh-quality parameter*

For the two-dimensional configuration analyzed in this study, the aerodynamic response is expressed through non-dimensional section coefficients. The lift coefficient is given by [20]:

$$C_L = \frac{2F_L}{\rho v^2 l} \tag{6}$$

The drag coefficient is given by:

$$C_D = \frac{2F_D}{\rho v^2 l} \tag{7}$$

where F_L is the lift force, F_D is the drag force, ρ is the fluid density, v is the freestream velocity, and l is the airfoil chord length.

The near-wall mesh quality is evaluated by the dimensionless wall parameter y+, defined as [21]:

$$y^+ = \frac{\rho u_\tau y_P}{\mu} = \frac{u_\tau y_P}{\nu} \tag{8}$$

where u_τ is the friction velocity, y_P is the distance from the wall to the center of the first cell, μ is the dynamic viscosity, and ν is the kinematic viscosity.

The aerodynamic efficiency of the system is assessed through the ratio C_L/C_D but its interpretation must be supported by the corresponding flow-field visualizations, especially in cases where stronger loading is accompanied by larger wake formation and flow separation.

3. COMPUTATIONAL DOMAIN

There are several commonly used CFD packages considered for this type of analysis, namely ANSYS Fluent, COMSOL Multiphysics, and OpenFOAM. In this case ANSYS Fluent was selected as the most suitable solver for the present research because it offers a strong balance between precision, capability for complex simulations, and practical usability [22]. The analyzed configuration consists of two NACA 6412 airfoils arranged in tandem. The leading edges of the airfoils are separated by $A = 170$ mm in the streamwise direction and $B = 30$ mm in the transverse direction (Figure 1).

The chord length of each airfoil is $l = 200$ mm. The position of the elements is kept identical for all investigated cases, while the angle of attack of the second, variable airfoil is changed to $-15°$, $-20°$, and $-25°$ (Figure 1).

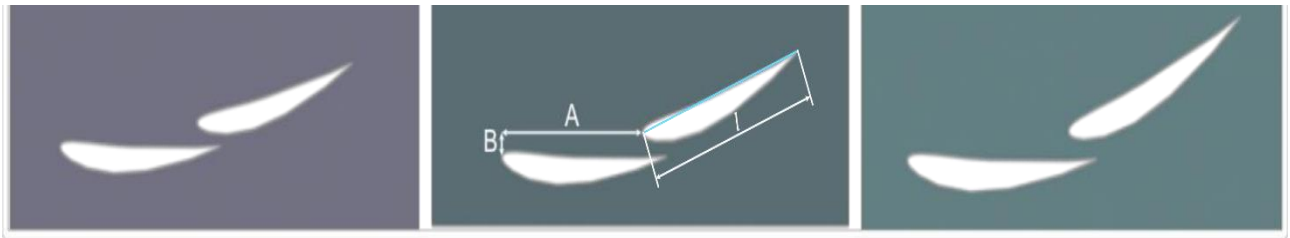

(a) (b) (c)

Fig. 1. Geometric definition of the tandem NACA 6412 configuration with A = 170 mm, B = 20 mm, and chord length l = 200 mm, under –15° (a), –20° (b), and –25° (c).

Since the configuration can be treated with a constant spanwise behavior, the analysis is carried out in a two-dimensional domain. The fluid domain was constructed in SolidWorks and sized according to the characteristic parameters proposed for double-element airfoil analysis [23]. The domain dimensions were defined so that: $C = 50 \cdot l$ and $D = 60 \cdot l$, as it can be seen on Figure 2. A rectangular subdomain of $3 \cdot 0.8\,m$ was additionally introduced around the airfoil system in order to enable local mesh refinement in the region of primary interest.

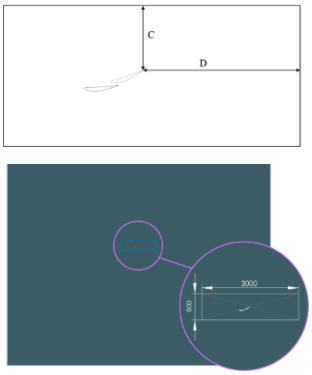

Fig. 2. Computational domain and local refinement region used for the tandem airfoil simulations.

3.1. *Mesh generation and near-wall treatment*

The computational domain was discretized using an unstructured triangular mesh. The mesh-generation procedure included: definition of the global maximum cell size, refinement of the rectangular zone around the profiles, edge division along the airfoil contours, introduction of inflation layers, and final mesh generation. Three mesh densities were initially tested in order to determine an appropriate balance between computational cost and accuracy. The dense mesh used a maximum element size of 0.1 m, the medium mesh 0.25 m, and the coarse mesh 0.6 m. The differences in the resulting values of C_L and C_D supported the selection of the medium mesh as an adequate compromise for the remaining simulations, as the differences were in the order of 10^{-3}, as it is depicted in Table 1.

T a b l e 1

Mesh selection analysis results

Type of mesh	Maximum elements size (m)	C_L	C_D
Fine	0.1	0.0925	–3.068
Medium	0.25	0.0928	–-3.069
Coarse	0.6	0,0928	–3.065

To ensure accurate near-wall resolution, the first boundary-layer cell height was set to $0.00002\ m$, the inflation region consisted of 15 layers, and the growth factor was 1.18. The mesh was designed so that the final simulations would retain $y^+ < 1$, which is suitable for resolving the near-wall region in the present study (Figure 3) [24].

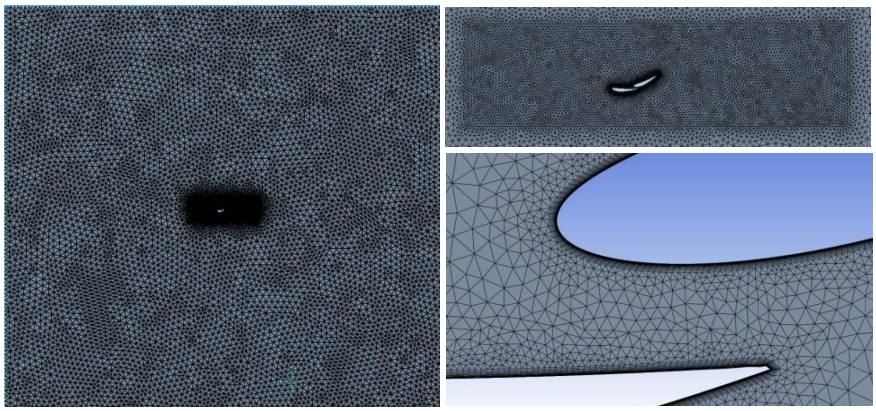

Fig. 3. Final discretization of the fluid domain

3.2. *Boundary conditions and simulation cases*

The boundary conditions were defined through inlet, outlet, fluid zone, wall boundaries, and the boundary layer around the airfoils. The outlet was prescribed through pressure-outlet conditions equal to atmospheric pressure.

The simulations were carried out at standard atmospheric pressure: $p_{atm} = 101325$ Pa and temperature: $T = 288.15$ K, for air with a density $\rho = 1.2250$ kg/m^3 and dynamic viscosity $\mu = 1.7894 \cdot 10^{-5}$ Pa·s. Only the flow field was of interest, therefore the energy equation was not included in the solution procedure.

The processing stage was carried out through 500 iterations for each of the nine cases. The residuals and monitored output parameters showed stabilization after approximately 150 iterations. Although literature may suggest lower continuity residuals as ideal, the residual level on the order of 10^{-4} obtained in this study was treated as acceptable for the intended engineering interpretation [25].

T a b l e 2

Operating cases of all performed simulations

Case number	v_{inlet} (m/s)	α (°)
1	11.11	
2	16.67	–15
3	22.22	
4	11.11	
5	16.67	–20
6	22.22	
7	11.11	
8	16.67	–25
9	22.22	

4. RESULTS AND DISCUSSION

4.1. *Numerical results*

The averaged numerical results obtained from ANSYS Fluent are summarized in Table 3. The table includes the lift coefficient, drag coefficient, wall parameter y^+, and the reported C_L/C_D ratio for all nine cases. The numerical data show that the absolute value of the lift coefficient increases as the angle of attack of the variable airfoil is increased from $-15°$ to $-25°$. At the same time, the drag coefficient also increases. This indicates that stronger aerodynamic loading is accompanied by stronger viscous phenomena. The largest magnitude of the lift coefficient is obtained at $v = 22.22\,m/s$ and $\alpha = -25°$, however, the **highest efficiency** is at the same velocity but at a lower angle of attack of $\alpha = \mathbf{-15°}$ (see highlighted data in Table 3). This shows the flow complexity and that higher lift does not correlate to overall higher efficiency.

An important outcome of the simulation is that all y^+ values remain below 1. The values vary between approximately 0.52 and 0.99, which confirms that the near-wall discretization was sufficiently refined for all simulated cases. As the velocity and the angle of attack increase, y^+ also tends to increase, which is consistent with the expectation of stronger gradients and more intense near-wall flow behavior.

Table 3

Numerical results for the tandem airfoil system

Velocity (m/s)	AOA (º)	Lift coefficient C_L	Drag coefficient C_D	y^+	C_L/C_D
11.11	–15	–3.0677023	0.092479007	0.52106687	–33.17187759
	–20	–3.6163794	0.11618891	0.53262596	–31.12499635
	–25	–3.8712711	0.15007215	0.5248618	–25.79606609
16.67	–15	–3.1142081	0.085772302	0.75516411	–36.30785262
	–20	–3.6736985	0.10732995	0.76528352	–34.22808359
	–25	–3.9461482	0.13926282	0.75589286	–28.33597797
22.22	–15	–3.1453805	0.081071928	0.9752026	–38.79740593
	–20	–3.7153239	0.10126909	0.99018781	–36.68763983
	–25	–4.0031303	0.13169004	0.97874969	–30.39812502

The original interpretation of the combined numerical and graphical results retained the $-25°$ configuration as the preferred arrangement. However, the numerical results alone are not sufficient for a final conclusion. For that reason, the flow field visualizations are essential for understanding whether the stronger aerodynamic loading is accompanied by undesirable wake growth and flow detachment.

4.2. *Velocity field*

The velocity contours provide the first direct insight into the aerodynamic behavior of the tandem configuration. For all investigated cases, shown in Figure 4, the velocity beneath the airfoils is higher than above them, which is consistent with the generation of a downforce. This is the key mechanism responsible for the downward aerodynamic loading of the system.

As the angle of attack of the variable airfoil increases, the flow behavior becomes progressively less attached near the trailing edge of that element. This effect is especially evident at the largest angle of attack, where a clear separation region appears behind the second airfoil. The tendency becomes even more pronounced as the freestream velocity increases.

The velocity contours therefore reveal two simultaneous tendencies. First, higher angle of attack increases the loading capability of the system. Second, the same increase promotes separation and wake formation. This means that the most aggressively loaded configuration also becomes the most vulnerable to aerodynamic losses generated by the disturbed downstream flow.

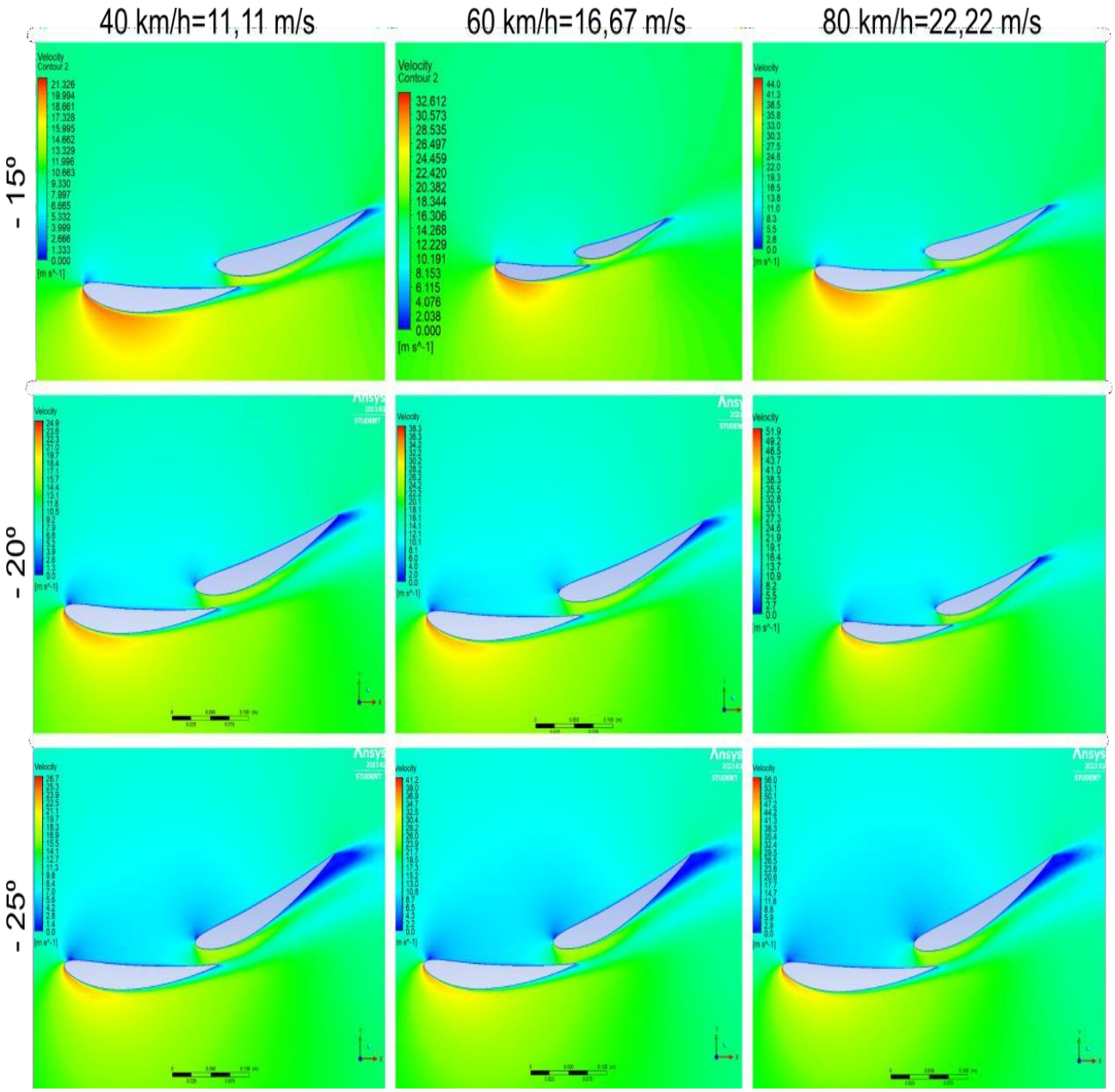

Fig. 4. Velocity contour distribution around the tandem airfoil system for the investigated inlet velocities and angles of attack

4.3. *Pressure distribution*

The pressure contours and pressure-distribution diagrams are consistent with the velocity field, as it can be observed in Figure 5. In accordance with Bernoulli-type interpretation of the flow, regions of higher local velocity coincide with reduced pressure, while the opposite occurs in regions of slower motion. Strong pressure differences are observed near the leading edges of both airfoils and along their surfaces.

The pressure field confirms that the airfoil pair produces substantial downward loading. At the same time, the pressure plots also indicate the onset of disturbed flow at the trailing edge of the variable airfoil. In the largest-angle cases, particularly at $-25°$, the pressure field shows stronger mixing between higher and lower pressure zones in the wake region. This is a clear sign of increasingly turbulent and separated flow.

Therefore, while the pressure gradients support stronger negative lift at higher angle of attack, they also highlight the aerodynamic cost of that choice. The pressure field does not simply confirm improved loading, but it also reveals the mechanism by which wake structures become stronger.

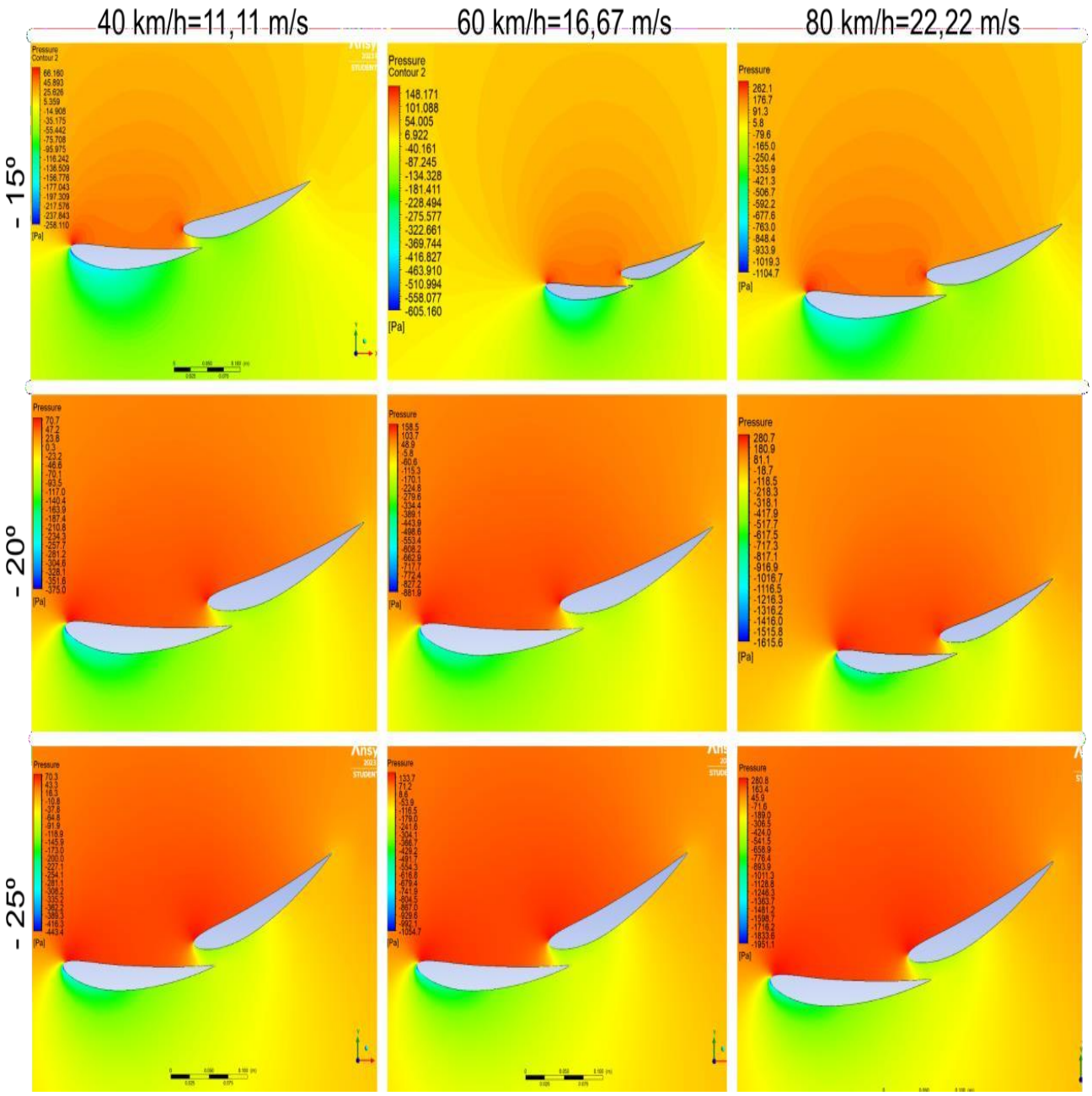

Fig. 5. Pressure contour distribution and surface-pressure behavior around the tandem airfoil system.

4.4. *Turbulent kinetic energy, streamlines, and velocity vectors*

The turbulent kinetic energy (TKE) contours in Figure 6 provide the clearest evidence of the wake intensity generated by the variable airfoil. The highest TKE values are concentrated behind the second airfoil, and the concentration becomes stronger as the angle of attack is increased.

In the wake region, the local velocity decreases strongly while the turbulent kinetic energy becomes large. This combination indicates the presence of intense turbulent structures immediately downstream of the variable element. The largest turbulence concentration is observed in the $-25°$ cases, where the trailing-edge separation is most visible.

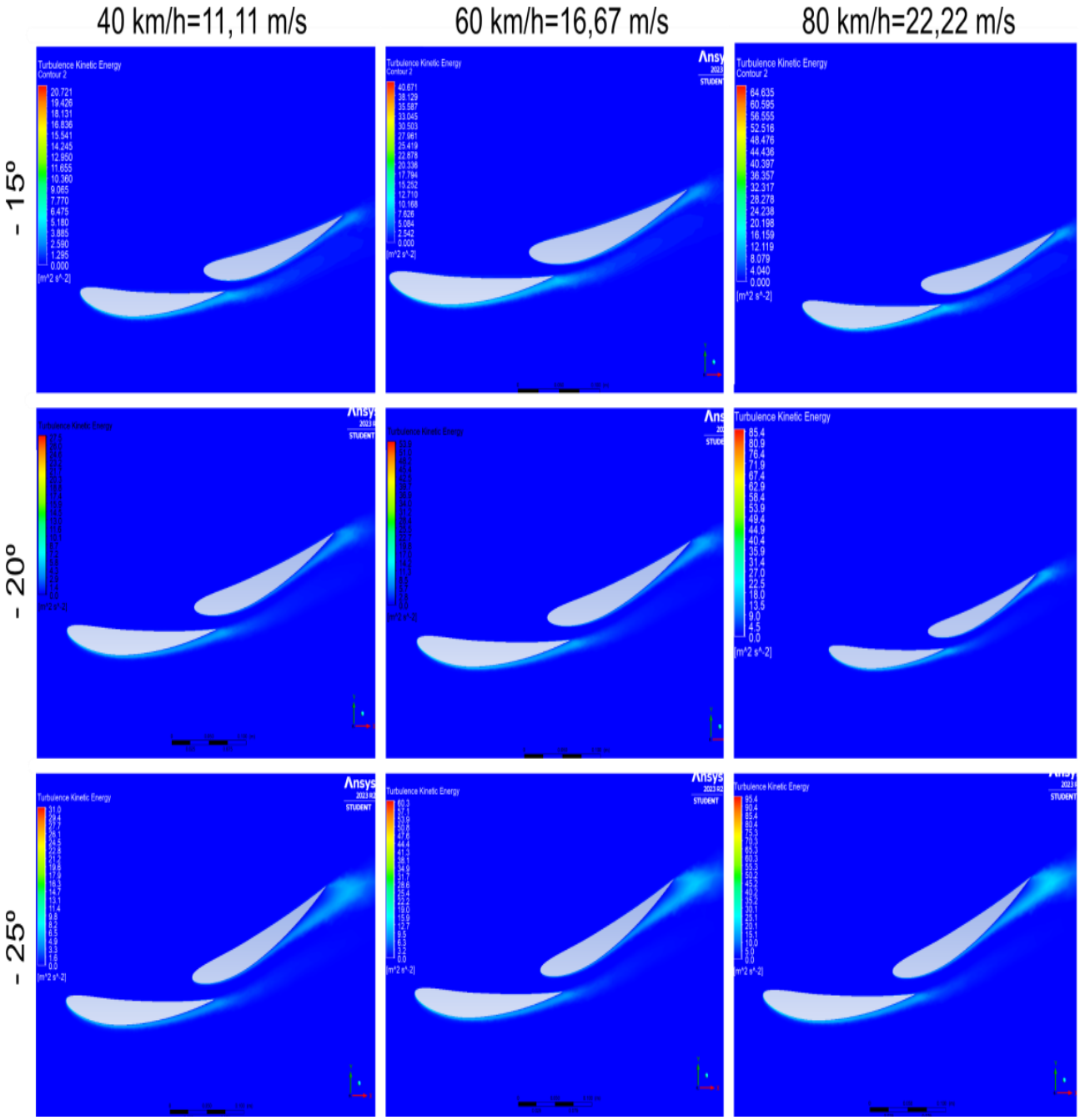

Fig. 6. Turbulent kinetic energy contours around the tandem airfoil system

In a streamline analysis shown in Figure 7, this was also visualized support the same conclusion. At higher angles of attack, the streamlines detach from the contour of the variable airfoil instead of following its surface smoothly. The velocity-vector plots additionally show the direction and local organization of the separated flow. The most pronounced vortex is observed for the case with $v = 22.22$ m/s and $\alpha = -25°$, where the wake structure behind the trailing edge is clearly developed.

Taken together, the graphical results show that the $-25°$ configuration is associated with the strongest aerodynamic loading but also with the largest wake, strongest turbulence, and clearest evidence of flow separation. This is the central trade-off of the present study. The preferred configuration reported by the original thesis is therefore not a fully optimized final solution, but rather the most promising configuration within the investigated range, provided that further refinement is introduced to reduce the downstream wake. A two-dimensional

CFD analysis of a tandem configuration composed of two NACA 6412 airfoils has been presented. The study investigated the effect of the angle of attack of a variable second airfoil at three inlet velocities and evaluated the aerodynamic response through numerical coefficients and flow-field visualizations.

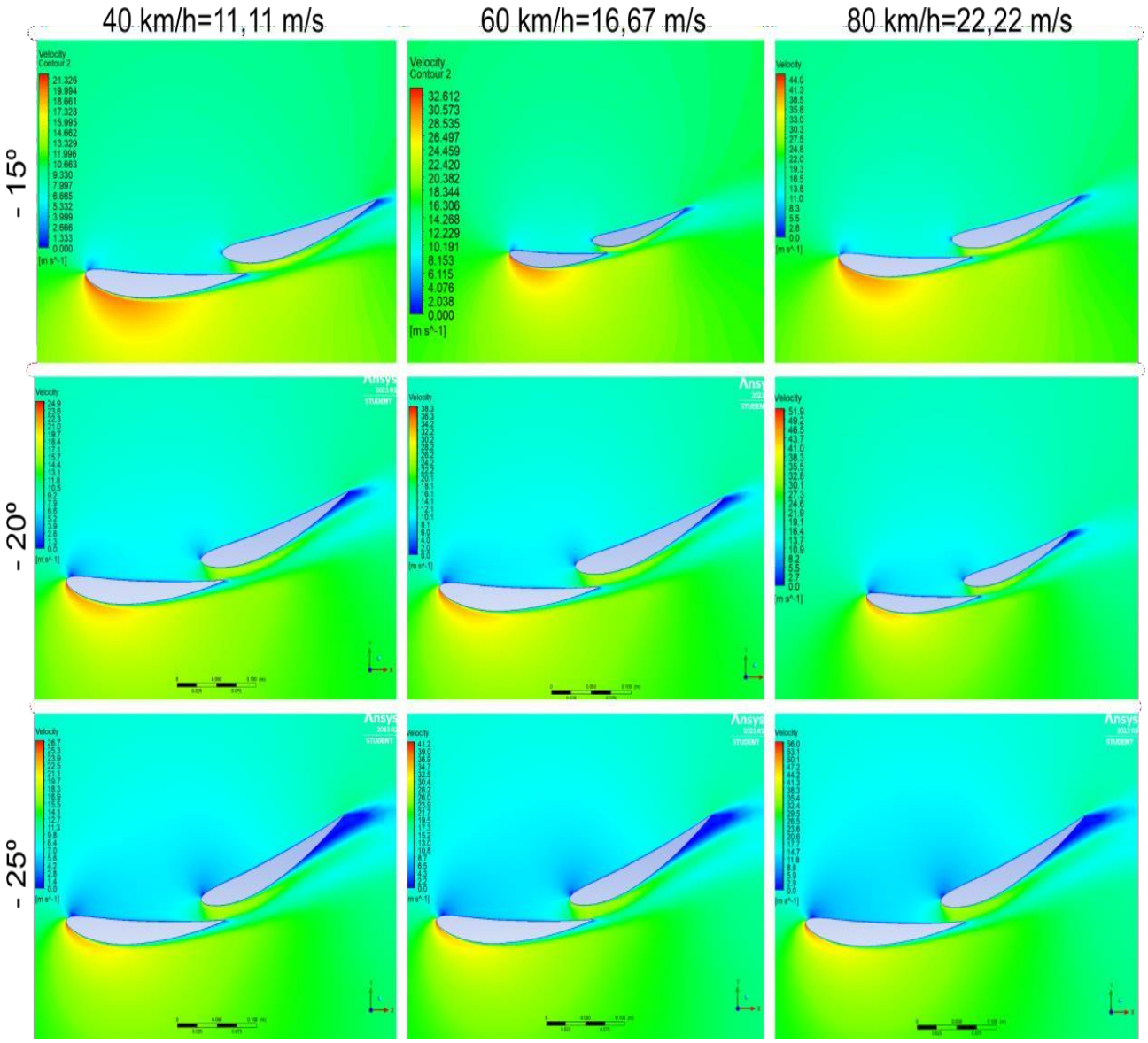

Fig. 7. Streamline contours based on velocity around the tandem airfoil system

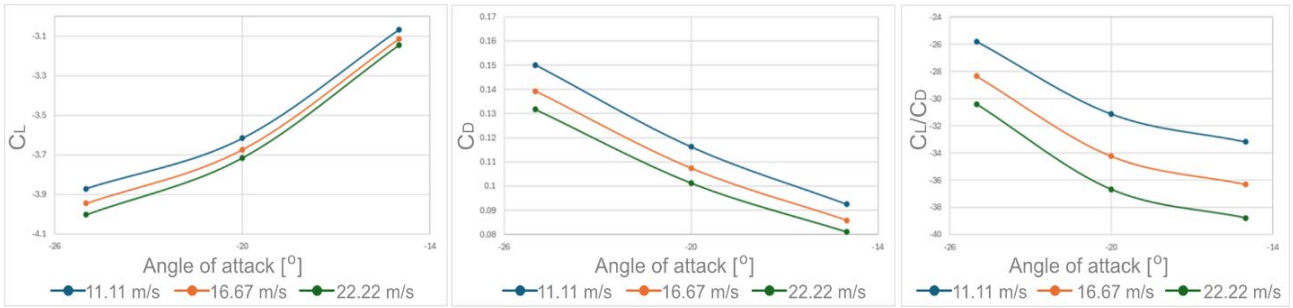

Fig. 8. Aerodynamic behavior within the tandem airfoil system, based on the a) lift coefficient, b) drag coefficient and c) efficiency ratio.

In Table 4 a representation of the change in lift drag and efficiency measure is reported. It can be noticed that with increase of the angle of attack, while the lift increases, the higher increase in drag lowered the overall efficiency for most cases. However, at higher velocities, hence at higher Reynolds numbers, this decrease of efficiency is less in all cases percentage-wise.

Table 4

Effects of changing the velocity and the angle of attack.

Velocity (m/s)	AoA (⁰)	Change in C_L (%)	Change in C_D %	Change in C_L/C_D %	Overall C_L/C_D change
11.11	–15				
	–20	17.9 ↑	25.6 ↑	6.2 ↓	
	–25	7.1 ↑	29. 2 ↑	17.1 ↓	28.6
16.67	–15				
	–20	17.97 ↑	25.1 ↑	5.7 ↓	
	–25	7.4 ↑	29.8 ↑	17.2 ↓	28.1
22.22	–15				
	–20	8.12 ↑	24.9 ↑	5.4 ↓	
	–25	7.75 ↑	30 ↑	17.1 ↓	27.6

5. CONCLUSION

The results show that increasing the angle of attack from -15° to -25° increases the magnitude of negative lift, but also increases drag and intensifies the wake behind the variable airfoil. The y^+ values remains below 1 in all nine cases, confirming satisfactory near-wall resolution and supporting the numerical reliability of the simulations.

The graphical analysis demonstrated that the most severe separation, largest turbulent kinetic energy, and strongest vortex structures occur in the -25° configuration, particularly at the highest investigated velocity. Nevertheless, based on the combined numerical and graphical interpretation presented in the original study, the -25° arrangement was retained as the preferred configuration among the three investigated angles. On another note, it was observed that at higher velocities, the increase in angle of attack is less significant when it comes to efficiency. Both the lift and drag coefficients increased, but due to the higher increase of drag, the overall efficiency always decreased.

The main conclusion is that the aerodynamic behavior of the tandem system is governed by a balance between stronger loading and stronger wake development. For that reason, the selected configuration should be understood as a promising basis for further optimization rather than a final solution. Future work should therefore be directed toward more advanced three-dimensional simulations and toward the introduction of additional aerodynamic elements capable of reducing separation and controlling the wake development without reaching stall conditions, as all performance would be compromised.

REFERENCES

[1] Blazek, J. (2001): *Computational Fluid Dynamics: Principles and Applications*, Alstom Power Ltd., Baden-Daettwil, Switzerland.

[2] Lazarevikj, M., Stojkovski, F., Iliev, I., Markov, Z. (May 2019): Influence of the guide vanes design on stress parameters of Francis 99 turbine, Third Francis 99 Workshop, NTNU, Trondheim, Norway, *Journal of Physics: Conference Series*, Volume 1296, 012008, https://doi.org/10.1088/1742-6596/1296/1/012008

[3] Rumsey, C. L., Ying, S. X. (2002): Prediction of high lift: review of present CFD capability, *Journal of Progress in Aerospace Sciences*, vol. **38**, no. 2, pp. 145–180, https://doi.org/10.1016/S0376-0421(02)00003-9,

[4] Lazarevikj, M., Stojkovski, F., Markov, Z., Iliev, I., Dahlhaug, O. G. (2022): Parameter based tool for Francis turbine guide vanes design using coupled MATLAB –

ANSYS approach, *J. Sustain. Dev. Energy Water Environ. Syst*., Vol. **10**, Iss. 3, 1090410, DOI: https://doi.org/10.13044/j.sdewes.d9.0410

[5] Crochet M. J. (1989): Numerical simulation of viscoelastic flow: a review, *Rubber Chemistry and Technology*, vol. **62**, no. 3, pp. 426–455. DOI:10.5254/1.3536253

[6] N.N.: What is CFD | Computational Fluid Dynamics?, SIMSCALE, https://www.simscale.com/docs/simwiki/cfd-computational-fluid-dynamics/what-is-cfd-computational-fluid-dynamics/

[7] Hall, N.: Guide to Aerodynamics, NASA, https://www1.grc.nasa.gov/beginners-guide-to-aeronautics/learn-about-aerodynamics/

[8] Fanjoy, D. and Dorney, D. (May 1, 1996): Numerical simulations of tandem-airfoil aerodynamics, *Aerospace Atlantic Conference & Exposition*, Dayton, Ohio, United States. https://doi.org/10.4271/961295.

[9] Delikan, M., Bal, Ş. (2025): A comprehensive CFD analysis of tandem foils with and without ground effect. *J Nav Archit Mar Technol*. **227** (1), pp. 1–21. DOI: 10.54926/jnamt.2025.247.

[10] Kryvokhatko, I. (2025): *Aerodynamics of Tandem Wing Aircraft*, 2nd edition,

[11] Fangzheng, C., Jianqiao, Y., Yuesong, M. (2017): Aerodynamic design optimization for low Reynolds tandem airfoil", Proceedings of the Institution of Mechanical Engineers, Part G. *Journal of Aerospace Engineering*, **232** (6): 095441001770421,

[12] Rajosik Adak et al. (2022): Aerodynamic performance of a tandem wing configuration inspired from dragonfly gliding flight for MAV application, Department of Aerospace Engineering, IIT Kharagpur.

[13] Anderson K. W. et al.: Navier-Stokes Computations and Experimental Comparisons for Multielement Airfoil Configurations, NASA Langley Research Center, Hampton, VA 23681, url: https://fun3d.larc.nasa.gov/papers/ja93.pdf

[14] Faure T. M. et al. (2017): Aerodynamic features of a two-airfoil arrangement, *Experiments in Fluids*. **58**, 146 https://doi.org/10.1007/s00348-017-2429-4

[15] Bikić, S., Todorović, B., Bukurov, M., Radojčin, M., Pavkov, I. (2018): Accuracy analysis of air torque position dampers based on blade profiles and damper locations, *Therm. Sci*. **22** (1B), 675–685. https://doi.org/10.2298/TSCI160805174B

[16] Chaiyanupong, J., Khajorntraidet, C. (2024): Design and analysis of double element airfoil using RANS, *Journal of Research and Applications in Mechanical Engineering*, vol. **12**, no. 1. Paper No. JRAME-24-12-003.

[17] N. N.: Ansys Fluent - Fluid Simulation Software, ANSYS, https://www.ansys.com/products/fluids/ansys-fluent

[18] N. N.: K-Epsilon Turbulence Models, SIMSCALE. https://www.simscale.com/docs/simulation-setup/global-settings/k-epsilon/

[19] Launder, E., Sharma, B. I. (1974): Application of the energy dissipation model of turbulence to the calculation of flow near a spinning disc, *Letters in Heat and Mass Transfer*, vol. **1**, pp. 131–138.

[20] N. N.: What is Lift Coefficient?, SIMSCALE. https://www.simscale.com/docs/simwiki/lift-drag-pitch/what-is-lift-coefficient/

[21] N. N.: Y-Plus Application in CFD Simulation, MR CFD. https://www.mr-cfd.com/y-plus-application-in-cfd-simulation/

[22] N. N.: Top Computational Fluid Dynamics (CFD) Software, Technology Evaluation Centers. https://www3.technologyevaluation.com/c/computational-fluid-dynamics-cfd

[23] Anderson, J.: Fluids – Lecture 19: Airfoils – Overview, MIT. https://web.mit.edu/16.unified/www/FALL/fluids/Lectures/f19.pdf

[24] N. N.: Calculators and Tools, FluidMechanics101. https://www.fluidmechanics101.com/pages/tools.html

[25] Stern, F., Wilson, R. V., Coleman, H. W., Paterson, E. G. (1999): *Verification and Validation of CFD Simulations*, Iowa Institute of Hydraulic Research & Propulsion Research Center, Mechanical and Aerospace Engineering Department, University of Alabama in Huntsville.